Extreme Wildfire Events Data Hub for Improved Decision Making

Union Civil Protection Mechanism (UCPM) call KNOWLEDGE FOR ACTION IN PREVENTION AND PREPAREDNESS, UCPM-2023-KAPP-PREP, Project number: 101140363

Deliverable tittle	**Report on simulations of extreme wildfires**
Contributing WP	WP 4 - Data processing and analysis
Dissemination level	Public
Contractual delivery date	31/12/2025
Actual delivery date	
Editor	Chiel van Heerwaarden (WU)
Contributors	Tristan Roelofs (WU), Martin Janssens (WU), Jordi Vilà-Guerau de Arellano (WU), Marc Castellnou (CFRS)

Document history			
Version	**Date**	**Modifications**	**Source**
D_v.1	08/12/2025	First draft	WU
R_v.1		Review	NIPV, PCF
F		Final version	WU

Table of Contents

List of Figures

List of Acronyms

EWED	Extreme Wildfire Events Data Hub for Improved Decision Making
LES	Large-Eddy Simulations
MicroHH	3D simulation tool
SCQ	Santa Coloma de Queralt

Intentionally blank

Executive Summary

This report describes the insights acquired into wildfire behaviour and interactions between fire and meteorology as acquired from 3D simulations with MicroHH. The case study from which this is derived is the first day of the Santa Coloma de Queralt fire (Catalunya, Spain, 24th of July 2021), during which a balloon sounding was made. The report is a summary of the extensive work that has been submitted to the scientific journal Atmospheric Chemistry and Physics [1]. A preprint of this paper is already online and can be consulted if more extensive information is desired.

In summary, the study demonstrates that the MicroHH simulation tool [3] successfully captured the key features of the observed wildfire plume and provides enhanced insight into the plume's behavior. Detailed examination of the airflow patterns reveals strengthened rear inflow driven by pyro-convection, alongside a frontal inflow of similar strength, forming part of a fire-driven circulation pattern upstream of the fire front. This frontal inflow has the potential to offset the intensified rear inflow and is linked to fire-generated vortical structures and distant ember transport. Furthermore, the analysis shows that the fire-induced circulation concurrently deepened and compressed the boundary layer up to 4 km ahead of the fire, thus interfering with the normal evening transition from a convective daytime boundary layer to a stably stratified nocturnal one. This interference offers a credible mechanism for the persistent nighttime combustion observed during the Santa Coloma de Queralt fire. Consequently, the authors propose propose that the principal influence of pyro-convection on wildfire dynamics hinges on the interplay between airflow patterns behind and ahead of the fire (modified hypothesis), rather than depending exclusively on the intensification of rear inflow (initial hypothesis).

1. Introduction

1.1. Overview

Extreme wildfires occur when fire behavior surpasses the firefighting capacity, which is, among others, the case when the fire line intensity exceeds 10 MW m^{-1} [1], triggering strong upward convection (pyro-convection) that alters surrounding winds. These modified winds affect fire behavior, creating a feedback loop called wildfire-atmosphere interactions, associated with unpredictable fire spread. Recent extreme events in Spain (2021) and Portugal (2017) spread much faster than predicted and unexpectedly burned through the night. The Santa Coloma de Queralt (SCQ) fire in Catalonia on July 24, 2021 (see Figure 1 for an overview), spread up to 4 times faster than expected by the local fire analysts and maintained a convective plume until midnight, making it a valuable case study as a rare extreme event with both documented fire behavior and measured pyro-convection.

Current operational fire models exclude pyro-convection impacts due to poorly understood physical mechanisms. Potter [5],[6] proposed that pyro-convective updrafts increase upwind surface inflow, potentially explaining accelerated fire spread. While turbulence-resolving Large-Eddy Simulations (LES) have the ability to complement the sparseness of observations by simulating pyro-convection in 3D space and time, realistic LES studies of past wildfires remain difficult to validate due to limited measurements during dangerous conditions. Most studies validate against fire perimeters or ambient weather, which does not ensure accurate pyro-convection simulation.

This study develops an observation-driven LES of the SCQ fire using in-plume sounding measurements from the Catalan Fire and Rescue Service, enabling validation of simulated pyro-convection through thermodynamic plume structure comparison. The objectives are to: (1) demonstrate LES capability to reproduce in-plume observations during extreme wildfires; (2) study pyro-convection's impact on surrounding wind patterns; and (3) analyze fire-driven winds' effects on atmospheric boundary layer thermodynamic structure. MicroHH, a proven turbulence-resolving LES tool, is utilized, as it enables landscape-scale domains (~10 km) at high resolution (~10 m), allowing simulation of both large-scale ambient turbulence and small-scale plume structures.

1.2. Description of the fire

The SCQ fire (see Figure 1a) ignited on July 24, 2021 at 14 UTC and spread eastward under westerly winds, rapidly developing a convective plume. Between 17-19 UTC, occasional overshooting created short-lived overshooting pyrocumulus clouds (oPyroCu), followed by a sea breeze arrival at 19 UTC (see Figure 1c). After 19 UTC, no further pyroclouds formed as atmospheric stabilization during the day-to-night transition likely limited the plume's vertical extent, preventing it from reaching the lifting condensation level. However, the fire maintained a dry convective plume until midnight (22 UTC), despite cooling and moistening around sunset (19:41 UTC).

At 19:51 UTC, a sounding released at the fire's right flank (see Figure 1b) measured vertical profiles of temperature, relative humidity, and rising speed starting from 80 m above ground level. Rising speeds exceeding the ambient maximum of ±2 m s^{-1} indicated the sounding captured the convective plume between 0.2-1.4 km altitude during ascent. A partial environmental profile was also measured during descent around 20:30 UTC, enabling validation of both the simulated convective plume and ambient environment.

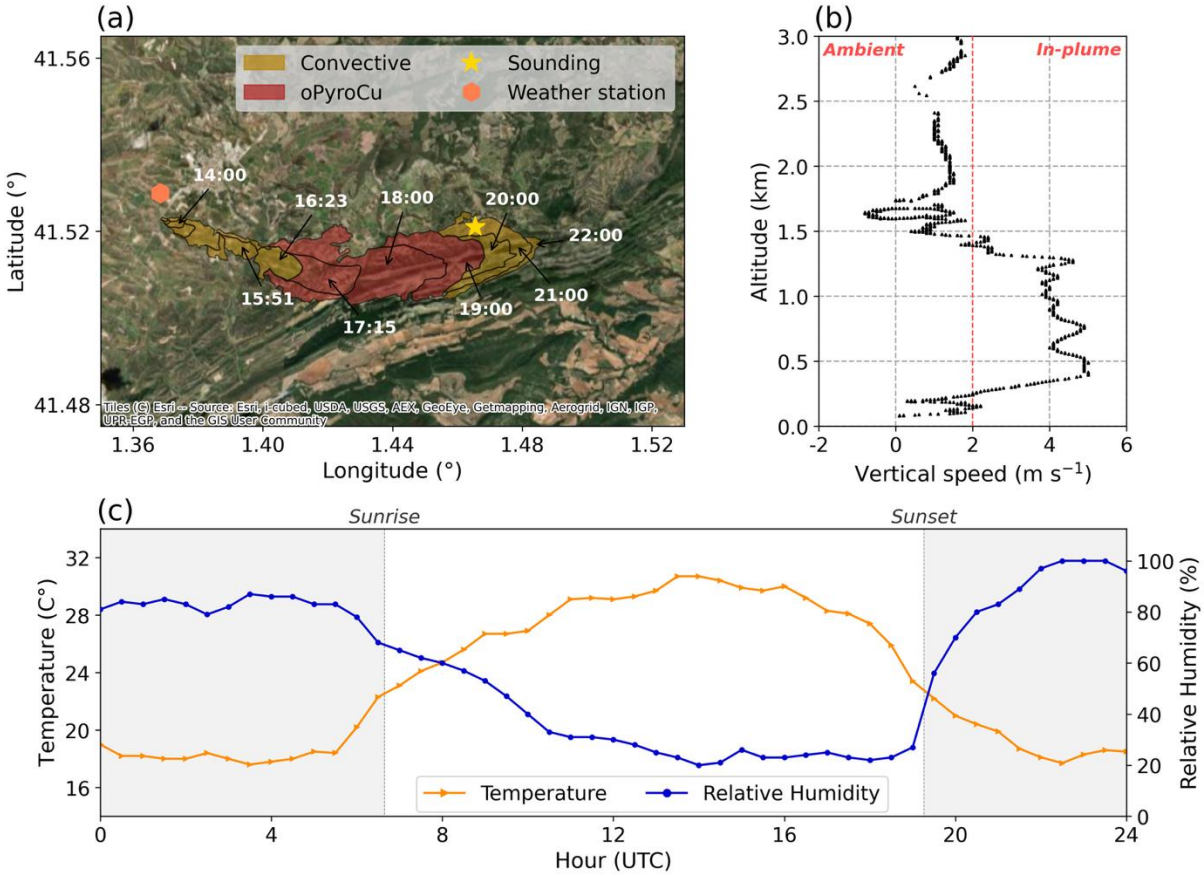

Figure 1. (a) Fire spread during the first day of the SCQ fire in UTC (LT - 2), including the locations of the sounding (star) and the synoptic weather station (hexagon). (b) The rising speed of the sounding that is used to determine whether a sounding is in or outside the convective plume based on a 2 m/s threshold (red dotted line). (c) The diurnal evolution of the temperature and relative humidity measured by the synoptic weather station.

2. Methods

This study prioritizes atmospheric realism while simplifying fire behavior to isolate pyro-convection's atmospheric impact. We performed two four-hour simulations (16-20 UTC) with MicroHH [3]: one without fire and one with fire. The difference reveals the SCQ fire's impact. Analysis focuses on 19-20 UTC, matching the sounding measurement time (19:51 UTC). The first two hours serve as spin-up, after which the fire is initialized, allowing an additional hour for plume development.

ERA5 reanalysis data provide boundary conditions for realistic meteorology. The data indicates sea breeze arrival after 16 UTC (moistening and backing winds), transforming the convective boundary layer at 16 UTC, that is heated from the surface, into a wind-driven neutral boundary layer capped by a residual layer at 19-20 UTC, coinciding with the shift from positive to negative surface heat flux. The domain measures 38.4 km × 25.64 km × 12 km (elongated eastward to prevent plume recirculation) with 25 m horizontal and stretched vertical resolution starting at 10 m. The fire is implemented as a moon-shaped surface area (1100 m × 150 m) with 145 kW m^{-2} sensible heat flux, based on estimations from people in the field, emitting an inert tracer for visualization.

Two key simplifications: (1) stationary fire (justified by the observed rate-of-spread being slower than the near-surface wind speeds); (2) prescribed ERA5 surface fluxes (negating radiation scheme and plume shadowing, negligible at sunset). These simplifications reduce complexity while enabling the main objective: assessing pyro-convection's atmospheric impact.

3. Results

3.1. Validation

To validate the simulated pyro-convection between 19 and 20 UTC, the simulated vertical profile of the virtual potential temperature (θ_v) is compared with observations (see Figure 2). The in-plume sounding measurements show that between 0.4 and 1.4 km in height, a relatively constant θ_v of 308 K is observed within the convection plume (where rising speed > 2 m/s). Above this well-mixed layer, an inversion is found at 1.7–1.9 km with a stable layer on top (> 1.9 km). The same inversion and stable layer are captured during the sounding's descent, which measured environmental conditions. Therefore, to validate the simulated plume, the observed vertical profile of θ_v during the ascent between 0.4 and 1.4 km is compared with the simulated θ_v inside the convection column.

The observations are compared with the median θ_v profile (blue line in Figure 3b) inside the average simulated convection column, with spread indicated by the first and third quantiles (blue dotted lines). For consistency, the same approach validates the simulated environment, using the reference run (without fire) and the median based on the entire xz cross-section.

Figure 2b shows the median θ_v profile inside the average convection plume up to 2.3 km. At the surface, the median θ_v reaches 384 K (not shown), which quickly decreases due to mixing with colder ambient air (304 K). This contrasts with sounding observations (black triangles), which show decreasing θ_v near the surface because the simulated profile starts inside the flaming zone, whereas the sounding was launched outside at the left flank. Above this rapid decrease, a well-mixed layer with θ_v varying between 307 and 310 K matches the observed 308 K (black triangles). However, the inversion capping this layer is simulated ±0.3 km higher than observed (1.7 km). The same difference appears in the environment (Figure 2a).

The environmental conditions are based on ERA5 boundary conditions, which also overestimate the inversion height by 0.3 to 0.4 km. Hence, the mismatch originates from ERA5. This overestimation is consistent with measurements by Mangan et al. [4], who showed ERA5 consistently overestimates convective boundary layer height due to its inability to capture local surface heterogeneity, resulting in overestimated residual layer height at night. The overestimated inversion height likely causes the simulation to overestimate plume height, potentially amplifying pyro-convection's impacts on the surrounding environment. However, this is not expected to significantly alter this study's outcomes, as the objective is to explore the physical mechanisms behind pyro-convection's impacts on atmospheric kinematic and thermodynamic structure.

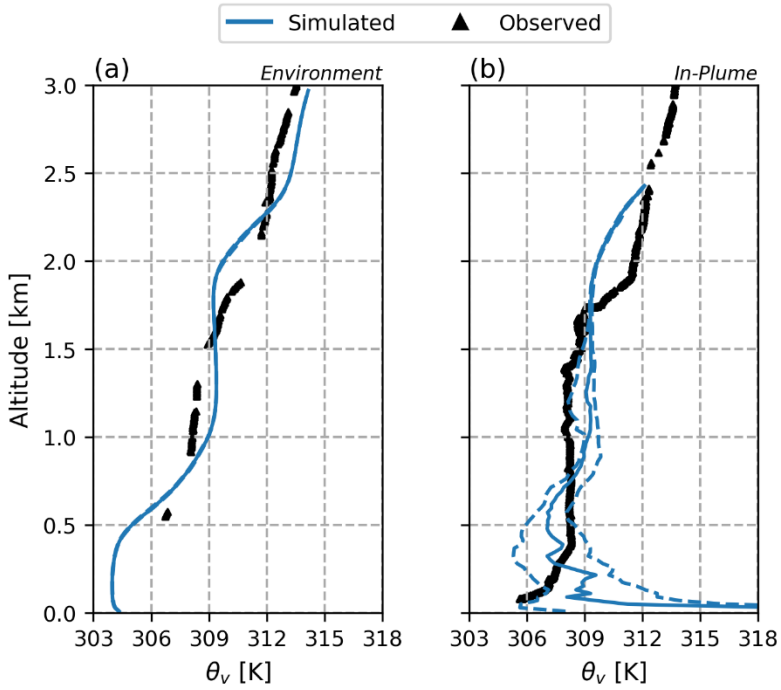

Figure 2. The vertical profiles of virtual potential temperature measured during the descent (environment) and ascent (in-plume) of the sounding compared to the median simulated in the average environment (a) and the average convection plume (b) between 19 and 20 UTC. The first and third quantiles (blue dashed lines) indicate the simulated variability.

3.2. Flow patterns modification caused by fire plume circulation

We compare the simulation with the fire with the simulation without to investigate how the fire impacts its surrounding wind patterns. We find that the fire creates strong buoyancy through atmospheric heating, producing vertical velocities up to 3 m s^{-1} at the surface (Figure 3b), which is an order of magnitude larger than the environmental vertical velocities (Figure 3a). To sustain this increased vertical airflow above the flaming zone (indicated by the black dotted line in Figure 3b), additional horizontal inflow into the flaming zone is required. We identify two mechanisms providing this additional inflow: (1) downdrafts at the southern borders of the flaming zone and (2) horizontal inflow from the western, eastern, and northern borders, as shown by the grey streamlines.

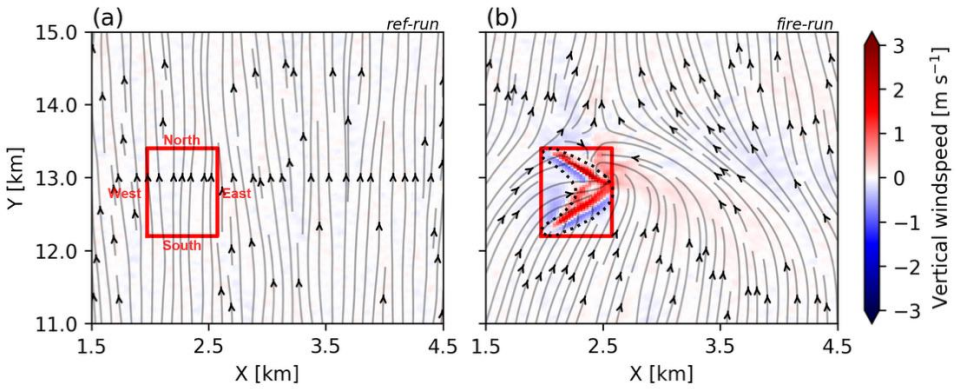

Figure 3. Circulation (streamlines) close to the land surface (10 m height) under conditions of a) no fire and b) fire conditions between 19 and 20 UTC. Colours show the mean vertical wind speed, the square indicates the location of the wildfire.

We also examine the evolution of surface wind patterns with altitude through vertical cross-sections parallel to the eastward fire spread direction (Figure 4), which aligns with the observed plume development despite southerly surface winds. We find that both acceleration and deceleration of zonal winds extend up to 1.5 km altitude but with distinct patterns (Figure 4b): acceleration occurs primarily inside the plume (grey outline) with maximum values at the surface, while deceleration occurs mainly east of the fire (x > 2.6 km) with peak values between 0.5 and 1 km altitude. The vertical wind shows the largest acceleration inside the plume, reaching instantaneous speeds up to 32 m s^{-1}, and develops downdrafts ahead of the fire between x = 4-6 km extending to 1.2 km altitude (Figure 4d). The black streamlines (Figure 4a,c) reveal that these combined changes create a fire-induced circulation east of the SCQ fire, consisting of rising motions inside the plume, downdrafts 2 km ahead of the fire, and surface-level return flow. These airflow modifications suggest the SCQ fire altered the thermodynamic structure of the atmospheric boundary layer ahead of itself, potentially improving future burning conditions by entraining warmer and drier air towards the flames. This could explain the fire's continued spread until midnight.

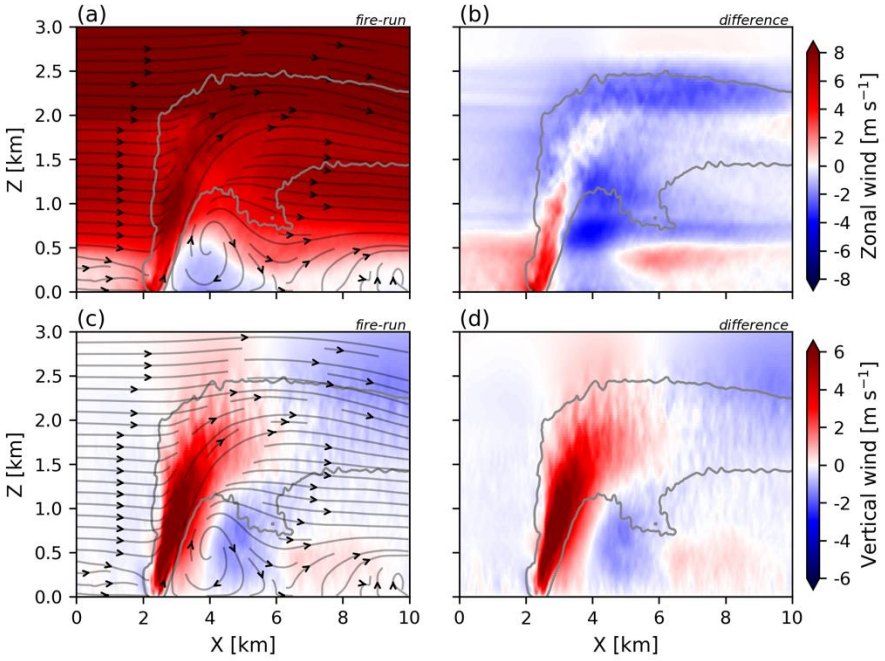

Figure 4. Vertical cross-sections of the average zonal (a) and vertical (c) wind between 19 and 20 UTC through the middle of the simulated fire. The grey outline and grey streamlines represent the average plume shape based on the inert tracer and the airflow through the cross-section. To visualise the acceleration and deceleration of the wind due to the fire, the average difference compared to no fire are shown for the zonal (b) and vertical (d) wind.

4. Conclusions

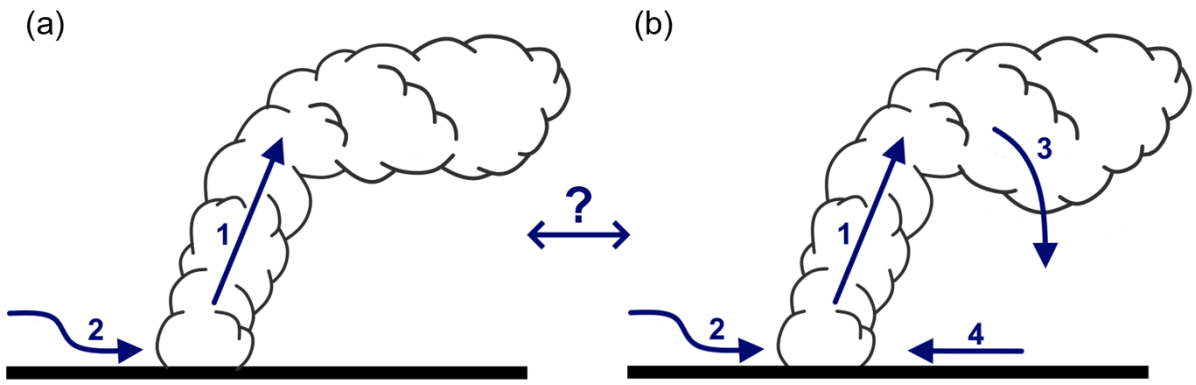

Figure 5. A schematic overview of the impacts of pyro-convection on the wind patterns following the paper of Potter (a) with (1) convective motions inside the plume and (2) accelerated and descending rear inflow, and an extended version based on the presented results here (b) including the fire-induced circulation, which consists of (1) convective motions inside the plume, (3) downdrafts ahead of the fire and (4) frontal inflow.

We demonstrated that the MicroHH simulation tool successfully captured the key features of the observed wildfire plume and enabled us to gain enhanced insight into the plume's behavior. Detailed examination of the airflow patterns revealed strengthened rear inflow driven by pyro-convection, alongside a frontal inflow of similar strength, forming part of a fire-driven circulation pattern upstream of the fire front. This frontal inflow had the potential to offset the intensified rear inflow and was linked to fire-generated vortical structures [7] and distant ember transport. Furthermore (shown in preprint), we observed that the fire-induced circulation concurrently deepened and vertically mixed the boundary layer up to 4 km ahead of the fire, thus interfering with the normal evening transition from a convective daytime boundary layer to a stably stratified nocturnal one. This interference offers a credible mechanism for the persistent nighttime combustion observed during the Santa Coloma de Queralt fire, where the fire is able to maintain sufficient convection to refresh the air near the fire. Consequently, we propose that the principal influence of pyro-convection on wildfire dynamics requires an updated view (see Figure 5) compared to earlier work: it hinges on the interplay between airflow patterns behind and ahead of the fire (modified hypothesis, Figure 5b), rather than depending exclusively on the intensification of rear inflow (initial hypothesis, Figure 5a).

This study paves the way for a deeper interpretation of fire plumes under a wide range of conditions and to better understand the interactions between plume turbulence and fire spread. Also, it helps understanding why there is often downward motions observed ahead of the fire resulting in a so-called “nose” in the smoke plume.

5. References

[1] Tedim, F., Leone, V., Amraoui, M., Bouillon, C., Coughlan, M.R., Delogu, G.M., Fernandes, P.M., Ferreira, C., McCaffrey, S., McGee, T.K. and Parente, J., 2018. Defining extreme wildfire events: Difficulties, challenges, and impacts. *Fire*, *1*(1), p.9.

[2] Roelofs, T., Castellnou, M., Vilà-Guerau de Arellano, J., Janssens, M. and van Heerwaarden, C., 2025. Wildfire-atmosphere interactions during the Santa Coloma de Queralt fire: the development of a fire-induced circulation. *EGUsphere*, *2025*, pp.1-29.

[3] Van Heerwaarden, C.C., Van Stratum, B.J., Heus, T., Gibbs, J.A., Fedorovich, E. and Mellado, J.P., 2017. MicroHH 1.0: A computational fluid dynamics code for direct numerical simulation and large-eddy simulation of atmospheric boundary layer flows. *Geoscientific Model Development*, *10*(8), pp.3145-3165.

[4] Mangan, M.R., Hartogensis, O., Boone, A., Branch, O., Canut, G., Cuxart, J., de Boer, H.J., Le Page, M., Martínez-Villagrasa, D., Miró, J.R. and Price, J., 2023. The surface-boundary layer connection across spatial scales of irrigation-driven thermal heterogeneity: An integrated data and modeling study of the LIAISE field campaign. *Agricultural and Forest Meteorology*, *335*, p.109452.

[5] Potter, B.E., 2012. Atmospheric interactions with wildland fire behaviour–I. Basic surface interactions, vertical profiles and synoptic structures. *International Journal of Wildland Fire*, *21*(7), pp.779-801.

[6] Potter, B.E., 2012. Atmospheric interactions with wildland fire behaviour–II. Plume and vortex dynamics. *International Journal of Wildland Fire*, *21*(7), pp.802-817.

[7] Lareau, N.P., Nauslar, N.J., Bentley, E., Roberts, M., Emmerson, S., Brong, B., Mehle, M. and Wallman, J., 2022. Fire-generated tornadic vortices. *Bulletin of the American Meteorological Society*, *103*(5), pp.E1296-E1320.